Shutdown dose rate measurements after the 2016 Deuterium-Deuterium campaign at JET

Shutdown Dose Rate Measurements after the 2016 Deuterium-Deuterium Campaign at JET

N. Fonnesu[a,b], R. Villari[a], S. Loreti[a], P. Batistoni[a], A. Klix[c] and JET Contributors[*]

EUROfusion Consortium, JET, Culham Science Centre, Abingdon, OX14 3DB, UK
[a] ENEA, Department of Fusion and Nuclear Safety Technology, I-00044 Frascati, Rome, Italy
[b] Department of Industrial Engineering, University of Rome 'Tor Vergata', 00133 Rome, Italy
[c] Karlsruhe Institute of Technology, 76344 Eggenstein-Leopoldshafen, Karlsruhe, Germany

The EUROfusion Work Package JET3 programme, established to enable the technological exploitation of the JET experiments over the next years, includes, within the NEXP subproject, a novel Shutdown Dose Rate (SDR) experiment. Considering its ITER-relevance, SDR experiment at JET represents a unique opportunity to validate the numerical tools for ITER nuclear analysis, through the comparison between numerical predictions and measured quantities (C/E). Within this framework, two active gamma dosimeters based on spherical air-vented ionization chambers (ICs) have been installed in ex-vessel positions close to the horizontal ports of the tokamak in Octants 1 and 2. The first JET campaign exploited in the novel SDR experiment is the latest 5-week Deuterium-Deuterium campaign (c36b), which achieved the best results in recent years in terms of high power operation. The present work is dedicated to the analysis of dose rate measurements carried out during this campaign and after shutdown. Proper correction factors are evaluated and applied to the instrument reading, while influence quantities and error sources are analyzed in order to calculate the overall experimental uncertainty.

Keywords: JET, Deuterium Campaign, Dose Rate in Fusion Experiments, Experimental Uncertainty in Dose Rate Measurement, Gamma Radiation Field in Fusion Experiments.

1. Introduction

The assessment of the shutdown dose rate (SDR) is a major safety issue for fusion devices, to guarantee the respect of dose limits to external exposure. SDR experiment at JET represents also a unique opportunity to validate the numerical tools for ITER nuclear analysis, through the comparison between numerical predictions and measurements. For this purpose, a novel SDR experiment has been included in the EUROfusion Work Package JET3 (NEXP subproject) to exploit the JET operation over the next years. The first campaign considered for this experiment is the Deuterium-Deuterium (D-D), held between October 10th and November 15th 2016. It has achieved the best results in recent years in terms of high power operation, with a total neutron yield > $9 \cdot 10^{18}$.
The present work is dedicated to the description of dose rate measurements carried out during the D-D campaign and after shutdown. As explained elsewhere [1], measurements are performed in terms of air kerma, which is equivalent to absorbed dose in air as long as the condition of charged particle equilibrium holds [2]. Signals acquired through the experimental equipment described in section 2 are converted into air kerma rate after a careful analysis of influence quantities affecting measurements, as detailed in section 3. Section 4 is dedicated to dose rate measurements and experimental uncertainty, conclusions are given in section 5.

2. Experimental equipment

The selected measuring equipment, described in [1], consists of two active gamma dosimeters for measuring the dose rate at the shutdown and during inter-shots. These are based on two 140 mm diameter air-vented spherical ionization chambers (ICs), PTW model 32002 [3], designed for radiation protection. They are characterized by excellent reproducibility, long-term stability and flat energy response in terms of air kerma. The PTW 32002 ICs are procured by ENEA and KIT (henceforth named respectively IC ENEA and IC KIT) and have been selected to cover a dose-rate range from background to 30 mSv/h (as predicted by calculations reported in [4]). A layout of the experimental assembly and data handling is shown in Fig. 1.

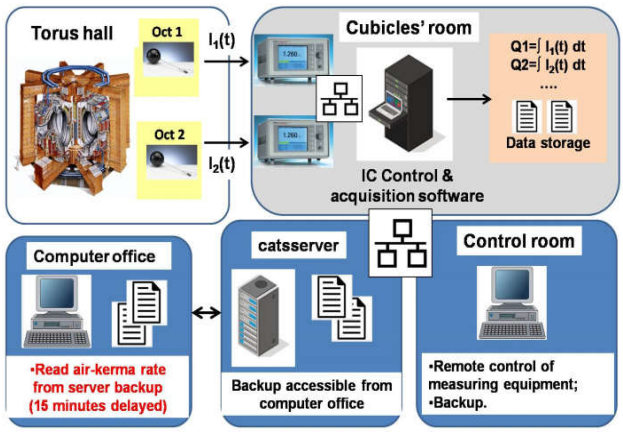

Fig. 1. Layout of the experimental assembly and data handling.

Two ex-vessel positions, close to the JET horizontal ports of Octants 1 and 2, have been selected for the location of ICs. The position in Octant 1 (IC ENEA) is close to the Radial Neutron Camera and the position in Octant 2 (IC KIT) is on the top of the ITER-like Antenna (ILA). ICs are operated in current mode and the output

author's email: nicola.fonnesu@enea.it
**See the author list of "Overview of the JET results in support to ITER" by X. Litaudon et al. to be published in Nuclear Fusion Special issue: overview and summary reports from the 26th Fusion Energy Conference (Kyoto, Japan, 17-22 October 2016)*

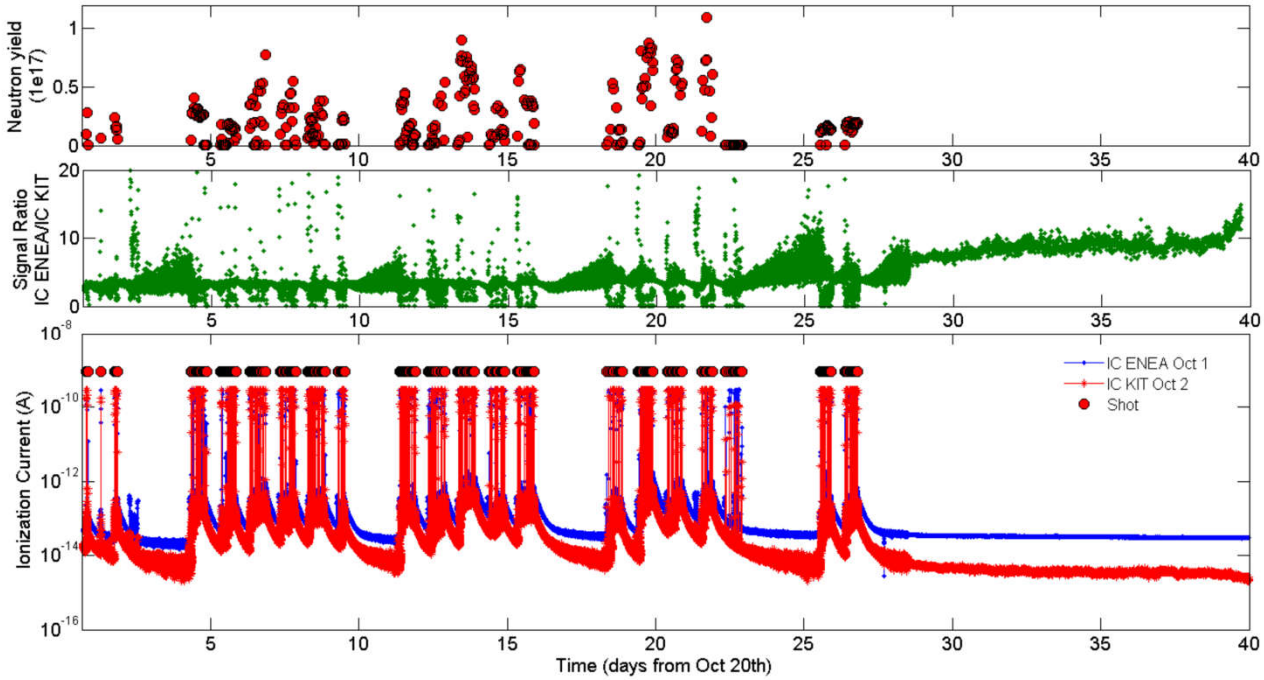

Fig. 2. (Color online) Bottom: signal (ionization current) measured by dosimeters during the first 40 days of SDR experiment; dots represent pulse times of the D-D campaign. Middle: signal ratio (IC ENEA to IC KIT). Top: neutron yield produced by JET pulses.

signal (ionization current) is read by two electrometers for dosimetry, model PTW UNIDOS [3]. They are equipped with an Ethernet interface for remote access through the laboratory local network (LAN). Ionization current, whose magnitude varies roughly from hundreds of pA (during inter-shots) down to tens of fA (after the campaign), must be preserved along a distance of about 100 m which separates ICs from electrometers. Low noise tri-axial cables serve as connection and provide insulated potentials for the measuring signal, the guard electrode, and high voltage to ICs (400 V). The measuring assembly and data acquisition are controlled from a PC located in the cubicles' room, by means of an ad hoc software developed by ENEA. It permits the remote control of electrometers through a TCP/IP connection, data handling and storage. The software gives also a complete instrument reading and some information related to the communication with electrometers. The computer in the cubicles' room can be accessed through the network from the JET diagnostic control room, thus enabling the control of the system also from there. Measurement data are backed up every 15 minutes to a JET server accessible from outside via remote connection.

3. From instrument reading to air kerma rate

Ionization current measured with the two dosimeters is shown in Fig. 2 (bottom) for the first 40 days of the experiment; red dots indicate pulse times. Neutron yield of each pulse, shown in the upper plot of the same figure, is calculated as time integral of neutron emissivity measured by JET neutron diagnostics. Electrometers are operated in low range mode, which means that a signal coming from ionization chambers larger than 275 pA is limited to this upper value. Signal ratio (IC ENEA to IC KIT) is displayed in the middle plot of Fig. 2; its value is about 5 and tends to increase at the end of pulses (when neutron emission ends), suggesting that the decay of the gamma radiation field in Octant 2 is faster than in Octant 1.

To obtain air kerma rate, ionization current I(t) is reduced by the average value of signal due to background radiation (I_{bkg}) and then integrated over a time interval Δt for calculating the collected charge Q(Δt):

$$Q(\Delta t) = \int_{t1}^{t1+\Delta t} \left(I(t) - \bar{I}_{bkg} \right) \cdot dt \qquad (1)$$

The average value of the charge collected in the ionization chamber per unit of time (Q/Δt) is proportional to the air kerma rate through the air kerma calibration factor N_K^{cal} :

$$\dot{K}_{air} = \frac{Q}{\Delta t} \cdot N_K^{cal} \qquad (2)$$

In order to have a good statistics for the calculation of the average value of the charge collected per unit of time (Q/Δt), the time interval Δt was set to 30 s during the campaign (when signal amplitude is about 100 pA) and increased to 600 s after shutdown (when the signal goes down to about 20-40 fA). The calibration of dosimeters at ENEA is described in [1]; here it is worth recalling that N_K^{cal} applies to a gamma radiation field with a broad-energy spectrum, and is calculated from calibration factors at different radiation qualities.

3.1 Quantities affecting instrument reading and correction factors

Precise and widely recognized codes of practice apply in the evaluation of influence quantities affecting dosimetric measurements and in the mitigation of their effects to a negligible level, e.g. see [5,6]. In the formalism introduced in such protocols, the instrument reading indicated as M_{raw} is the raw measurement to be corrected, which in our case is the charge collected per

unit of time (Q/Δt). A number of correction factors applies to this value to account for variations from the reference calibration conditions and to limit the effect of influence quantities. Among the corrections suggested by the IAEA and AAPM [5,6], the following correction factors are considered for the calculation of the corrected instrument reading M_{corr}:

$$M_{corr} = M_{raw} \cdot k_{TP} \cdot k_h \cdot k_{sat} \cdot k_{stab} \cdot k_{lin} \cdot k_{leak} \cdot k_{rot} \quad (3)$$

These factors are discussed in the following. Uncertainty related to the application of such corrections, is neglected if its (expanded) value is < 0.1%.

3.1.1 Air pressure and temperature (k_{TP})

The air mass in the cavity of a vented ionization chamber is affected by variations of temperature T_{IC} and pressure P_{IC}, which are the main responsible of air density variation (despite less significant, relative humidity may also play a role in this). Since the collected charge is proportional to the air mass inside the chamber, the correction that applies is the ratio of air density under reference standard conditions during calibration (i.e., T_0=293.15 K and P_0=1013 hPa) divided by the density of air during measurements. The correction factor k_{TP}, assuming that ideal gas law holds for the ambient air, takes the following form:

$$k_{TP} = \frac{P_0}{T_0}\frac{T_{IC}}{P_{IC}} \quad (4)$$

The calculation of k_{TP} has required monitoring temperature and pressure during the experimental campaign. No dedicated instruments have been provided for measuring air temperature and pressure near the two dosimeters in the JET torus hall and the only measurement of temperature available for air density correction (T_{HVAC}) comes from the ventilation system (HVAC) of the torus hall, whose diagnostics are integrated in the JET control and data acquisition system (CODAS).

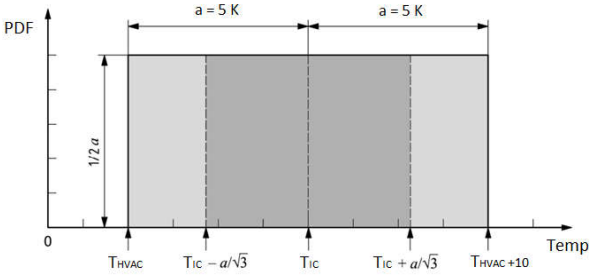

Fig. 3. Probability distribution function related to the air temperature measurement.

Considering the proximity of ICs to the tokamak, whose in-vessel components during operations are warmed up to about 300 °C, and that the thermometer of HVAC system is located far from it, the temperature of air inside IC cavity is estimated as T_{HVAC} + 5 K, within a uniform distribution limited by T_{IC} ± 5 K (Fig. 3). 5 K in terms of percentage value of T_{IC} (which is within the range 293-303 K), rounded to the first decimal, is 1.7%. As for P_{IC}, only a differential measurement of indoor pressure (with respect to the atmospheric pressure) is available from the barometer of HVAC system. For the estimation of the atmospheric pressure in Culham, records of the closest meteorological station (RAF Benson), provided by the UK's national weather service [7], are considered (P_{MET}). The expanded uncertainty related to this estimation is conservatively evaluated as ± 10 hPa (1.0% of P_{IC}) with a uniform distribution. In the calculation of P_{IC}, depression in the torus hall is neglected since its value, about 1.5 hPa, is irrelevant compared to the uncertainty on the atmospheric pressure. It follows that $P_{IC} = P_{MET} \pm 10$ hPa.

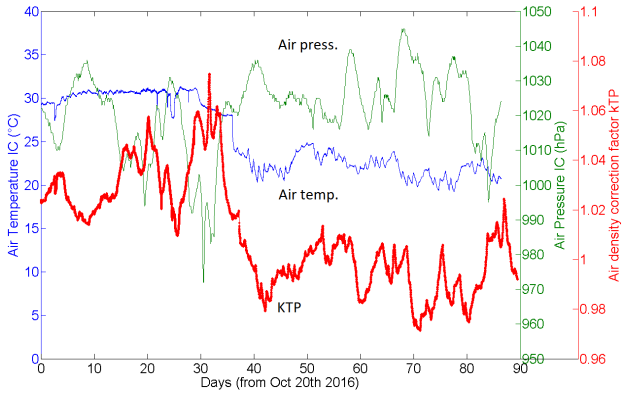

Fig. 4. Estimations of air temperature and pressure in the ionization chamber cavity and air density correction factor k_{TP}.

Temperature is recorded every 20 minutes, atmospheric pressure every hour; T_{IC} and P_{IC} at the times of dose measurement (i.e., every 30 s during campaign and 600 s after shutdown) are calculated with linear interpolation (Fig. 4). Errors associated to the assumption of linear variation of these quantities in such time intervals are negligible. As shown in Fig. 4, the correction due to air density variation during measurements is within 8%.

3.1.2 Humidity (k_h)

Humidity influences several parameters which play a role during calibration and dose measurement, such as air density, average energy for producing an ion pair and the mass stopping power for electrons [8]. These effects normally compensate each other so that the overall effect is smaller than single effects. In particular, the error introduced by ignoring variations in relative humidity (RH) in the range 20 to 80%, is within ± 0.15% of the reading [6,8]. RH is calculated from dew temperature (T_{dew}) records available from CODAS (HVAC diagnostics), by applying the Magnus formula [9]:

$$RH(\%) = 100 \cdot e^{\frac{a \cdot T_{dew}}{b+T_{dew}} - \frac{a \cdot T_{IC}}{b+T_{IC}}} \quad (5)$$

where a=17.625 and b=243.04. Accounting for the uncertainties introduced in the calculation of relative humidity by the Magnus formula (about 0.1%) and even more by the T_{IC} value (about 10%), RH is in the range 18-65%, and the above-mentioned error of ± 0.15% is reasonably applicable. For this, no correction is applied to M_{raw}, k_h = 1 and the (expanded) uncertainty is ± 0.15% (uniform distribution).

3.1.3 Ion recombination (k_{sat})

A small but measurable fraction of charges produced by the radiation field recombines before being collected and measured by dosimeters inducing a loss of signal. Since during the calibration of dosimeters at ENEA-INMRI

Table 1. Sources of uncertainty

Source of uncertainty	Correction factor	Expanded Uncertainty (%)	PDF	Type	Confidence Level (%)	Coverage Factor	$U(x_i)/xi$ (%)	Effective degrees of freedom (u_i)
Temperature	k_{TP}	1.70	rectangular	B	100	1.73	0.98	10
Pressure	k_{TP}	1.00	rectangular	B	100	1.73	0.58	10
Humidity	k_h	0.15	rectangular	B	100	1.73	0.09	30
Ion recombination	k_{sat}	neglected	-	-	-	-	-	-
Stability (IC)	k_{stab}	1.00	rectangular	B	100	1.73	0.58	100
Stability (elec.)	k_{stab}	0.10	rectangular	B	100	1.73	0.06	100
Linearity	k_{lin}	0.25	rectangular	B	100	1.73	0.14	100
Leakage current	k_{leak}	neglected	-	-	-	-	-	-
Tilting	k_{rot}	5.00	rectangular	B	100	1.73	2.89	10
Rotation	k_{rot}	0.50	rectangular	B	100	1.73	0.29	30
Resolution	-	0.50	rectangular	B	100	1.73	0.29	30
Repeatability	-	0.25	normal	B	68	1.00	0.25	30
Calibration factor	N_K^{cal}	2.04	normal	A	68	1.00	2.04	5

[10] the instrument reading was corrected for considering ion recombination (which means that the calibration coefficient N_K^{cal} applies to the instrument reading incremented for the recombination loss), the same correction coefficient must be applied before converting the signal into air-kerma. The correction factor considers the initial recombination P_{in} and the volumetric recombination dependent from the signal intensity P_{vol}:

$$k_{sat} = P_{in} + P_{vol} \cdot M_{raw} \quad (6)$$

For the dosimeter PTW 32002, P_{in} = 1.0013 and P_{vol} = 1174800 A^{-1}, as suggested by ENEA-INMRI. The magnitude of such correction is about 0.1-0.2%.

3.1.4 Stability (k_{stab}), linearity (k_{lin}), leakage current (k_{leak})

PTW certifies that the variation of the response of dosimeters to the same identical radiation field is ± 1% per year for the ionization chambers and ± 0.1% per year for the electrometer [3]. Considering that IC calibrations date back to more than one year ago and correcting instrument reading for long-term stability would require a new calibration (to evaluate the variation of the response to the same input after one year), such uncertainties (with uniform distribution) are accounted for, and no correction is applied (k_{stab}=1).

The manufacturer certifies also that neglecting the non-perfect linearity of instrument reading, a maximum error of ± 0.25% the reading value should be considered. Perfect linearity is assumed (k_{lin}=1) and the mentioned error included in the uncertainty budget.

Polarizing voltage applied to ICs is responsible of a small leakage current (usually less than 0.1% of ionization current) inside the ionization chambers and in the cable, also present in the absence of radiation. Before starting dose rate measurements, the average value of ionization current due to the background radiation in the torus hall (I_{bkg}), which also includes leakage current, has been measured and then subtracted from I(t) during SDR measurements. For this reason, under the hypothesis of constant leakage current, such effect has already been removed from M_{raw} and no correction factor is needed. Uncertainty on this correction is reasonably supposed to be < 0.1% and it has been neglected.

3.1.5 Direction of radiation field (k_{rot})

Dosimeters, calibrated under a reference radiation field perpendicular to their longitudinal axis, are exposed to a complex gamma radiation field made of several sources and impinging dosimeters from many directions, mainly on their upper half-sphere. Considering the complexity of such field, a dedicated experiment for assessing a correction factor for the field geometry would be extremely difficult. In lack of this, no correction is applied (k_{rot}= 1) and the variation of the dosimeter response due to the angular dependence is accounted in the uncertainty budget. From the dosimeter's manual, such dependence is within ± 5% for tilting the longitudinal axis with respect to the perpendicular field and ± 0.5% for rotation around the same axis.

4. Dose rate measurements

Once the instrument reading is corrected for influence quantities and M_{corr} calculated, air kerma rate is obtained by applying Eq. 2, which following the formalism of dosimetric protocols reads:

$$\dot{K}_{air} = M_{corr} \cdot N_K^{cal} \cdot k_{Q,Q0} \quad (7)$$

$k_{Q,Q0}$ is a factor to account for the difference in beam qualities during calibration (Q_0) with respect to the measured radiation field (Q). Considering the peculiarity of SDR experiment, where a radiation field with a broad energy spectrum is measured (while protocols essentially refer to mono-energetic beams) such factor is not directly applicable. As explained in [1], the energy dependence of the dosimeter response was measured during their calibration and the uncertainty on the calibration coefficient N_K^{cal} takes into account this effect. Air kerma rate measurements in Octant 1 and Octant 2 during D-D campaign and up to two months after shutdown are shown in Fig. 5. As earlier mentioned, the measuring range of electrometers is the lowest allowed and peaks observed in correspondence of JET pulses are

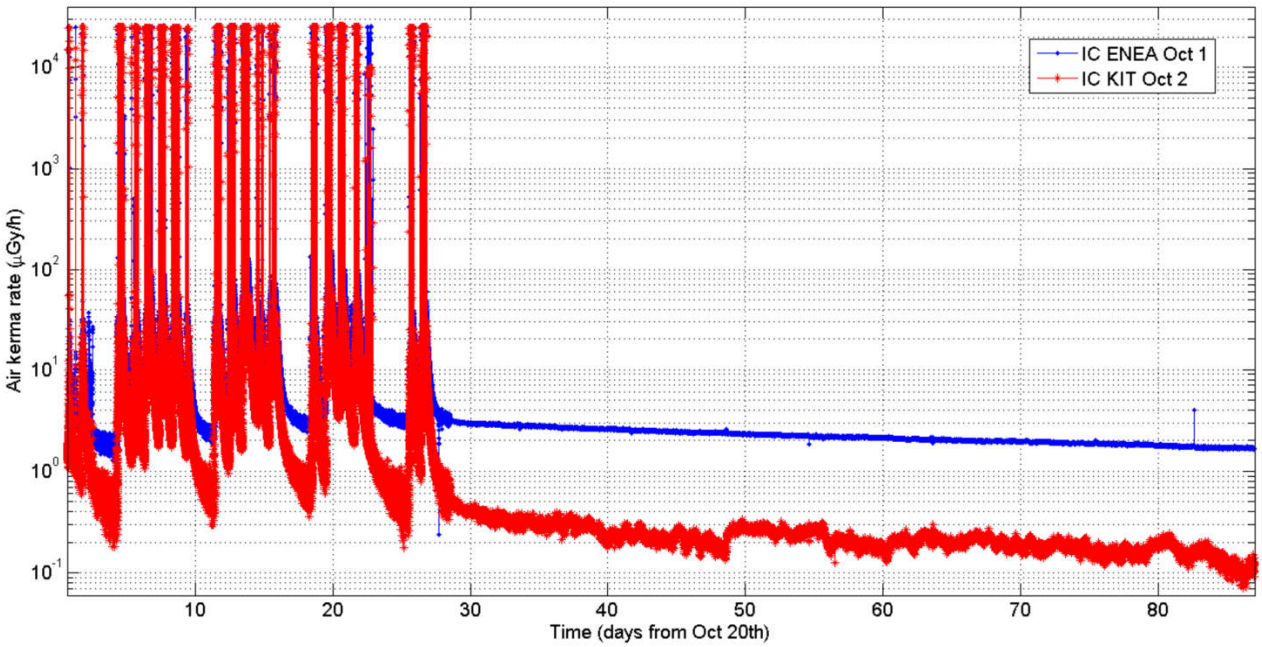

Fig. 5. (Color online) Air kerma rate measurements during D-D campaign and up to two months after shutdown.

limited to the air kerma rate value corresponding to 275 pA. To follow the entire pulse evolution, it would be necessary to change measuring range from medium or high (during the pulse) to low (after the pulse end), introducing a dead time of few seconds in the change of scale. This is avoided since the experiment aims at measuring the gamma decay after neutron emission. After shutdown IC in Octant 2 reached the lower limit of the measuring range in less than 20 days, while exponential decay in Octant 1 is measured for more than two months. A detailed discussion on these measurements is given elsewhere [11].

Identifying gamma emitters through curve fitting of the SDR decay curve, due to the high under-determination (type, number and activity of radionuclides), is difficult. The variable projection algorithm for the solution of nonlinear least squares problems [12] applied to the decay curve of IC ENEA, assuming 4 exponentials, converges to a local minimum in correspondence of the following equation (in μGy/h): $f(t) = 60.4e^{-13.3 \cdot t} + 31.5e^{-0.268 \cdot t} + 1.28e^{-0.0332 \cdot t} + 2.94e^{-0.0004 \cdot t}$. Three of these exponentials are close to Mn56 (whose decay constant is 0.268 h^{-1}), W187 ($2.91 \cdot 10^{-2}$ h^{-1}) and Co58 ($4.08 \cdot 10^{-4}$ h^{-1}), also detected by gamma spectrometry.

4.1 Experimental uncertainty

According to the ISO GUM recommendations for the calculation of measurement uncertainty [13], the overall uncertainty on SDR measurements is obtained by applying the error propagation formula to the expression of air kerma rate:

$$u^2_{\dot{K}air} = \sum_{i=1}^{N} \left(\frac{\partial \dot{K}_{air}}{\partial x_i} \right)^2 u^2(x_i) + 2 \sum_{i=1}^{N-1} \sum_{j=i+1}^{N} \frac{\partial \dot{K}_{air}}{\partial x_i} \frac{\partial \dot{K}_{air}}{\partial x_j} \cdot u(x_i, x_j) \quad (8)$$

Where u^2_{Kair} is the variance of air kerma rate and x_i is the generic input quantity with variance $u^2(x_i)$. The second term of the right-hand side of Eq. 8 is due to correlation of some input quantities. In our case, relative humidity and T_{IC} are correlated (Pearson's correlation coefficient is r=-0.84) and it would imply a correlation between k_{tp} and k_h. However, since k_h has been assumed constant, the uncertainty in the value of T_{IC} does not affect k_h. Considering the simple multiplicative form of the expression of air kerma rate and the absence of correlation of input quantities, the relative uncertainty of air kerma rate can be written on the basis of Eq. 8 as the root of the sum of squared relative standard deviation of the input quantities:

$$\frac{u_{\dot{K}air}}{\dot{K}_{air}} = \sqrt{\sum_{i=1}^{N} \frac{u^2(x_i)}{x_i^2}} \quad (9)$$

Input quantities are reported in Table 1, together with their probability distribution functions (PDF) and effective degrees of freedom. In addition to uncertainties on the application of correction factors to the instrument reading described in the previous section, the digital resolution of the electrometer, repeatability and uncertainty on the calibration of dosimeter are also included in the uncertainty budget. Type A evaluation of standard uncertainty is based on a statistical analysis of repeated observations, while type B includes essentially scientific judgment and manufacturer's specifications [13]. The relative standard uncertainty of air kerma rate resulting from Eq. 9 is 3.8%.

4.2 Probability distribution function

To associate a confidence probability to the calculated standard deviation and to determine a coverage interval for a stipulated coverage probability, it is necessary to determine the probability distribution function of the air kerma rate. The ISO GUM approach for the determination of PDF is applicable whenever any dominant sources of uncertainty can be assumed to have a Gaussian distribution [13], and provided also that the relative uncertainty from each source is small, as usually occurs in dosimetry [14]. Under these circumstances, the

resulting (normalized) value of air kerma rate follows a t-distribution which approaches a standard Gaussian as the effective degrees of freedom of the combined uncertainty (ν_{eff}) grows up. Effective degrees of freedom (ν_i) for each source of uncertainty (type B) are evaluated according to the Bentley's work [14] and ν_{eff} calculated according to the Welch-Satterthwaite formula [13]. It follows that the normalized value of air kerma rate has a Student's distribution with ν_{eff} = 20. The conditions necessary for the applicability of such approach are not completely satisfied. Indeed, the dominant source of uncertainty is related to the dependency of the detector response from the direction of the incident radiation field, with a standard deviation of 2.9% and a rectangular PDF. The second source in terms of magnitude, due to the calibration of the instrument, has a Gaussian PDF with a standard deviation of about 2%. In order to understand "how far we are" from the conditions of applicability of the simplified approach and from the Student's (or Gaussian) distribution, the PDF of the air kerma rate is assessed numerically using Monte Carlo sampling. Such method, described in a supplement of the ISO GUM as "the propagation of distributions" [16], allows to determine the PDF of the result of a measurement by simulating the measuring process. A value of each input quantity drawn at random from its PDF, is used for the calculation of air kerma rate by applying the measurement model, i.e., equations 3 and 7. This process is then repeated a large number of times (trials) and the set of simulated results forms an approximation to the PDF for the value of air kerma rate. A dedicated code has been written in Fortran language [17] to propagate the distribution of input quantities. Two random number generators have been implemented in the code for simulating the extraction of numbers from rectangular (L'Ecuyer with Bays-Durham shuffle [18]) and Gaussian (the Box-Muller transform applied to the Park and Miller uniform number generator [18]) PDFs. Such algorithms, widely employed in scientific applications, passed the most relevant randomness tests and meet the standards required in the supplement of ISO GUM [16]. Simulations are performed with 10^6 trials, since seed-dependency is observable up to 10^5.

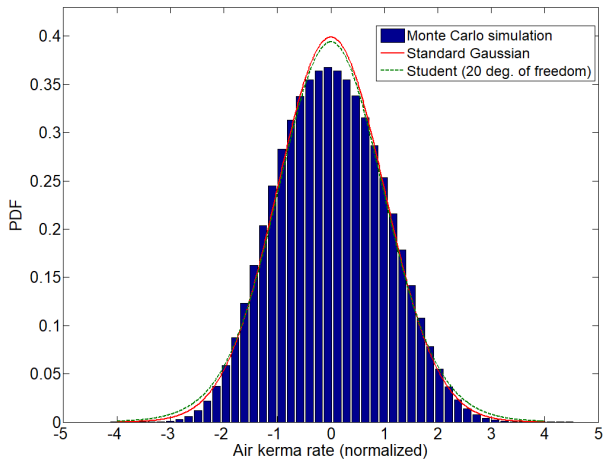

Fig. 6. Air kerma rate probability distribution function resulting from the propagation of distributions.

The air kerma rate, normalized with the mean and standard deviation follows the PDF shown in Fig. 6 and does not depend on the measurement point considered for its calculation. Student and standard Gaussian distributions are also plotted for comparison. A dominant rectangular uncertainty tends to spread the resulting PDF reducing the height of its peak. The standard deviation of 3.8% (calculated with the first-order error propagation law) has a confidence level of 65% in the PDF resulting from the Monte Carlo simulation, instead of 68% of the standard Gaussian. Considering the large number of sources of uncertainty of type B, which mainly come from judgements or manual's data, and the resulting level of reliability, the PDF distribution of air kerma rate can be approximated as a Gaussian; trying to distinguish between 65% and 68% makes no sense in such framework.

5. Conclusions and future work

Dose rate measurements with ionization chambers installed in Octant 1 and Octant 2 were performed at JET during the latest D-D campaign and after shutdown. The measuring equipment has shown a good temporal stability without drifts and significant perturbations due to harsh radiation conditions. The lack of a relevant signal degradation confirms that no damages were induced by neutrons. Measurements were analysed following precise dosimetry protocols (IAEA and AAPM), accounting for deviations of measuring conditions with respect to the calibration laboratory and influence quantities which affect instrument reading. Corrections applied, essentially due to the air density variation, are within 8% of the instrument reading. Other corrections are neglected since hardly estimable and the related uncertainty accounted in the uncertainty budget. Experimental uncertainties related to the SDR measurement were evaluated and quantified. The assessment of sources of uncertainties was carried out through measurements and statistical analysis (type A) and judgements and manual's data (type B). The ISO GUM approach for the determination of the distribution function of air kerma rate brings to a Student's distribution with 20 degrees of freedom. However, since the dominant source of uncertainty is rectangular, the applicability of such procedure was doubtful and it has required a more in-depth analysis through a Monte Carlo simulation of the measuring process. It has been found that the PDF of air kerma rate can be approximated as a Gaussian with a standard deviation of 3.8%.

The angular dependence of the dosimeter response to the incident radiation field is the major and most critical source of uncertainty. An improvement in the uncertainty analysis would be achievable in the future with the experimental measurement of such dependence and with a more precise measurement of air density near dosimeters. In view of the next Tritium campaign, the sensitivity of the dosimeters to the variation of the Oxygen content in the Torus Hall atmosphere (O2 percentage will be reduced to 15% for Tritium operations as a fire suppression preventative measure) will be investigated.

Acknowledgments

The authors are grateful to Joe Deane of CCFE for his valuable help in retrieving measurement data from JET CODAS and Massimo Pinto of ENEA-INMRI for his advice on how to quantify ion recombination inside ionization chambers.
This work has been carried out within the framework of the EUROfusion Consortium and has received funding from the Euratom research and training programme 2014-2018 under grant agreement No 633053. The views and opinions expressed herein do not necessarily reflect those of the European Commission.

References

[1] N. Fonnesu et al., The preparation of the Shutdown Dose Rate experiment for the next JET Deuterium-Tritium campaign, Fusion Eng. Des. (2017), http://dx.doi.org/10.1016/j.fusengdes.2017.01.030.
[2] International Commission on Radiation Units and Measurements (ICRU), Fundamental quantities and units for ionizing radiation, Journal of the ICRU **11** No 1 (2011) Report 85
[3] PTW Freiburgh GmbH. http://www.PTW.de, 2016 (accessed 01/07/2017).
[4] R. Villari, et al., Validation of shutdown dose rate Monte Carlo calculations through a benchmark experiment at JET, Fusion Eng. Des. 83 (2008) 1782.
[5] International Atomic Energy Agency (IAEA), Absorbed Dose Determination in External Beam Radiotherapy: An International Code of Practice for Dosimetry based on Standards of Absorbed Dose to Water, Technical Reports Series No. 398, IAEA, Vienna (2000).
[6] American Association of Physicists in Medicine (AAPM), AAPM's TG-51 protocol for clinical reference dosimetry of high-energy photon and electron beams. Med. Phys. 26 (9), September 1999, 1847-1870.
[7] The UK National Weather Service, http://metoffice.gov.uk (accessed 10/02/17).
[8] D.W.O. Rogers and C.K. Ross, The role of humidity and other correction factors in the AAPM TG-21 dosimetry protocol, Med. Phys. 15 (1), February 1988.
[9] O.A. Alduchov and R. E. Eskridge, Improved Magnus' form approximation of saturation vapor pressure, J. Appl. Meteor. 601–609 (35) 1996.
[10] The Italian National Institute of Ionizing Radiation Metrology (ENEA-INMRI). http://www.inmri.enea.it, 2016 (accessed 01/09/2016).
[11] R. Villari et al., **titolo paper di Sara** ,this conference.
[12]G. Golub and V. Pereyra, Separable nonlinear least squares: the variable projection method and its applications, Inverse Problems 19 (2003) R1-R26.
[13] International Organization for Standardization (ISO), Guide to the expression of uncertainty in measurement, ISO/IEC Guide 98-3, ISO, Geneva (2008).
[14] International Atomic Energy Agency (IAEA), Measurement Uncertainty. A practical guide for Seconday Standards Dosimetry Laboratories, IAEA-TECDOC-1585, IAEA, Vienna (2008).
[15] Bentley R.E., Uncertainty in Measurement: The ISO Guide, Monograph 1: NML Technology Transfer Series, National Measurement Laboratory, (Sydney 2003).
[16] International Organization for Standardization (ISO), Evaluation of measurement data - Supplement 1 to the "Guide to the expression of uncertainty in measurement" - Propagation of distributions using a Monte Carlo method, ISO/IEC Guide 98-3-1, ISO, Geneva (2008).
[17] International Organization for Standardization (ISO), Information technology - Programming languages - FORTRAN, ISO/IEC 1539-1:1997, ISO, Geneva (1997).
[18] William H. Press et al., Numerical Recipes in FORTRAN. The Art of Scientific Computing, Cambridge University Press, New York, New York (1993).